

Geophysical Research Letters

RESEARCH LETTER

10.1029/2020GL091271

Key Points:

- We developed tree-ring reconstructions of central U.S. soil moisture and the atmospheric ridge that causes flash droughts back to 1500 CE
- Observations capture flash drought's long-term probability distribution, but reconstructions reveal centennial fluctuations in variability
- Cycles in reconstructed atmospheric ridging may aid diagnosis and prediction of flash drought on interannual to decadal time scales

Supporting Information:

- Figure S1
- Figure S2
- Table S1

Correspondence to:

K. C. Bolles,
kbolles@ldeo.columbia.edu






Citation:

Bolles, K. C., Williams, A. P., Cook, E. R., Cook, B. I., & Bishop, D. A. (2021). Tree-ring reconstruction of the atmospheric ridging feature that causes flash drought in the central United States since 1500. *Geophysical Research Letters*, 48, e2020GL091271. <https://doi.org/10.1029/2020GL091271>

Received 13 OCT 2020
 Accepted 11 JAN 2021

© 2021. American Geophysical Union.
 All Rights Reserved.

Tree-Ring Reconstruction of the Atmospheric Ridging Feature That Causes Flash Drought in the Central United States Since 1500

Kasey C. Bolles¹ , A. Park Williams¹ , Edward R. Cook¹ , Benjamin I. Cook^{1,2} , and Daniel A. Bishop¹ 

¹Tree-Ring Laboratory, Lamont-Doherty Earth Observatory of Columbia University, Palisades, NY, USA, ²NASA Goddard Institute for Space Studies, New York, NY, USA

Abstract Rapid drought intensification, or flash droughts, is often driven by anomalous atmospheric ridging and can cause severe and complex impacts on water availability and agriculture, but the full range of variability of such events in terms of intensity and frequency is unknown. New tree-ring reconstructions of May–July mid-tropospheric ridging and soil moisture anomalies back to 1500 CE in the central United States—a hotspot for flash drought—suggest that over the last five centuries, anomalies in these two variables combined to indicate flash-drought conditions in ~17% of years and exceptionally severe flash drought in ~4% of years, similar to frequencies in recent decades. However, over one-third of all inferred exceptional flash droughts occurred since 1900, suggesting the 20th century was highly flash-drought prone. These results may guide future work to diagnose the roles of external, oceanic, and land-surface forcing of warm-season atmospheric circulation and hydroclimate over North America.

Plain Language Summary In 2012, the central United States experienced a “flash drought,” when rapid soil drying due to persistently low precipitation totals and high temperatures in late spring and summer caused billions of dollars in damages and agricultural losses. Such events are difficult to forecast because flash droughts can develop in a matter of weeks, and only a handful of flash droughts have been observed in recent decades, giving high uncertainty as to their likelihood. Here, we use tree rings to create two independent annual records of central United States soil moisture and the principal atmospheric circulation pattern known to cause flash droughts that extend back to the year 1500. Taken together, these records provide a new five-century perspective on these crucial components of flash drought and reveal for the first time the long-term behavior of central United States flash droughts, including frequency and cyclicity of exceptional events. We find that the instrumental record is a good representation of the long-term likelihood of flash droughts. This apparent agreement with long-term average conditions is largely by chance; however, as the reconstructions indicate large century-to-century variations in flash-drought frequency and magnitude over the past 500 years.

1. Introduction

Drought is one of the most challenging types of extreme weather to predict, posing a substantial challenge for a warming world in which much of the land surface is projected to experience more frequent and severe water deficits (Cook et al., 2020). The rapid onset and intensification of some droughts, termed flash droughts, catalyze devastating societal disruptions, such as that which occurred in the United States (U.S.) in 2012. This event impacted most of the contiguous U.S., producing the fourth largest spatial drought extent observed since 1895 and causing over \$30 billion in damages (Basara et al., 2019). Conditions were normal in May, but severe drought set in by July and arrived without early warning as seasonal forecasts failed to predict it (Hoerling et al., 2014). The persistent atmospheric ridging over central North America that drove the acute decrease in precipitation and soil moisture occurred in the absence of known large-scale drivers, such as sea surface temperature forcing (Basara et al., 2019; PaiMazumder & Done, 2016). The likelihood of such a severe event may have increased in recent decades, but any recent increase in the risk of exceptional summer flash droughts or the atmospheric ridging anomalies that promote them have not yet been assessed in the context of natural decadal variability (Hoerling et al., 2014). It is therefore critical

to develop long-term reconstructions of the atmospheric conditions that promote flash drought events to better understand the full range of such phenomena (Hoerling et al., 2014; Pendergrass et al., 2020).

Conventional drought in the U.S. can occur year-round, but flash drought preferentially occurs in warm months and over the central U.S. (Basara & Christian, 2018; Basara et al., 2019; Chen et al., 2019; Christian, Basara, Otkin, Hunt, et al., 2019; Christian, Basara, Otkin, Hunt, Wakefield, et al., 2019; Seager et al., 2019). Precipitation is the main driver of soil moisture variability in this region, with approximately 80% of annual totals falling in the warm season between April and September (Basara et al., 2013; Livneh & Hoerling, 2016). The atmospheric anomalies that drive warm-season precipitation anomalies in the extratropics are largely without clear teleconnections to sea-surface temperatures (Zhao et al., 2017), contributing to the lack of forecasting skill. Poor forecasting skill may also be caused by deficiencies in simulating seasonal-to-subseasonal circulation features, such as the identified quasi-stationary wave train that extends from the central north Pacific across North America and that sometimes places a strong and persistent summertime mid-tropospheric ridge over the central U.S. (Hodges & Pu, 2019; Seager et al., 2019; Wang et al., 2019; Zhao et al., 2017).

While slowly evolving drought conditions can develop without strong atmospheric ridging, ridging is a signature of the rapid development of flash drought events (Basara et al., 2019; Christian, Basara, Otkin, Hunt, Wakefield, et al., 2019; Christian et al., 2020; Koster et al., 2014; Pendergrass et al., 2020). The subsidence from an anomalous ridge inhibits convection and precipitation, elevates downwelling solar radiation and temperature, and lowers humidity (Cowan et al., 2017; Hodges & Pu, 2019; Lopez et al., 2019)—all recurring features of flash droughts (Christian, Basara, Otkin, Hunt, Wakefield, et al., 2019; Otkin et al., 2018; Pendergrass et al., 2020). Observation-based reanalyses of atmospheric circulation provide opportunities to learn more about the drivers of past ridging events, but these records are short and highly uncertain prior to the widespread availability of atmospheric soundings beginning in the 1960s and satellite data in the late 1970s.

With annual resolution, tree rings can provide a way to assess the severity and distribution of extreme single-year or multi-year drought events against slowly varying background states (Fritts, 1976; Pendergrass et al., 2020). North America is particularly well-represented by a network of thousands of ring-width chronologies, an established tool for climate reconstructions (e.g., E. R. Cook et al., 2010; Herweijer et al., 2006; Howard et al., 2018; Stahle et al., 2007). Though annual tree growth reflects more than the rate of the soil moisture dry-down that defines flash droughts, tree-ring reconstructions provide robust estimates of dry extremes in the Great Plains region (Woodhouse & Overpeck, 1998), and the geographic expanse of the tree-ring network across continents has proven useful for reconstruction of large-scale features of atmospheric circulation (E. R. Cook et al., 2019; Steiger et al., 2018; Wise & Dannenberg, 2014). For this study, we explore five centuries of central U.S. warm-season atmospheric ridging activity and concomitant regional soil moisture deficits reconstructed from tree rings. This novel pair of reconstructions elucidates the range of variability of flash drought-like conditions in a recognized geographic “hotspot” for such events and the potential for predictability of atmospheric anomalies that cause the rapid onset of drying.

2. Materials and Methods

2.1. Study Region and Season

We define the central U.S. as the region bound by 30°–47°N and 95°–105°W (Figure 1). Though flash drought can often be a sub-regional phenomenon, exploratory analysis revealed that warm-season soil moisture in this region varies strongly with mid-continental atmospheric ridging. The specific season of focus is May–July (MJJ) because this period coincides with the peak of the central U.S. seasonal precipitation cycle, the growing season, and the most common season of flash drought occurrence (Basara & Christian, 2018; Chen et al., 2019; Hoerling et al., 2014).

2.2. Climate and Hydrological Data for 1901 to 2020

We use gridded records of precipitation, vapor pressure deficit (VPD), and fraction of mean soil moisture (SMf) at 0.25° geographic resolution across North America for 1901–2020. SMf in a given month

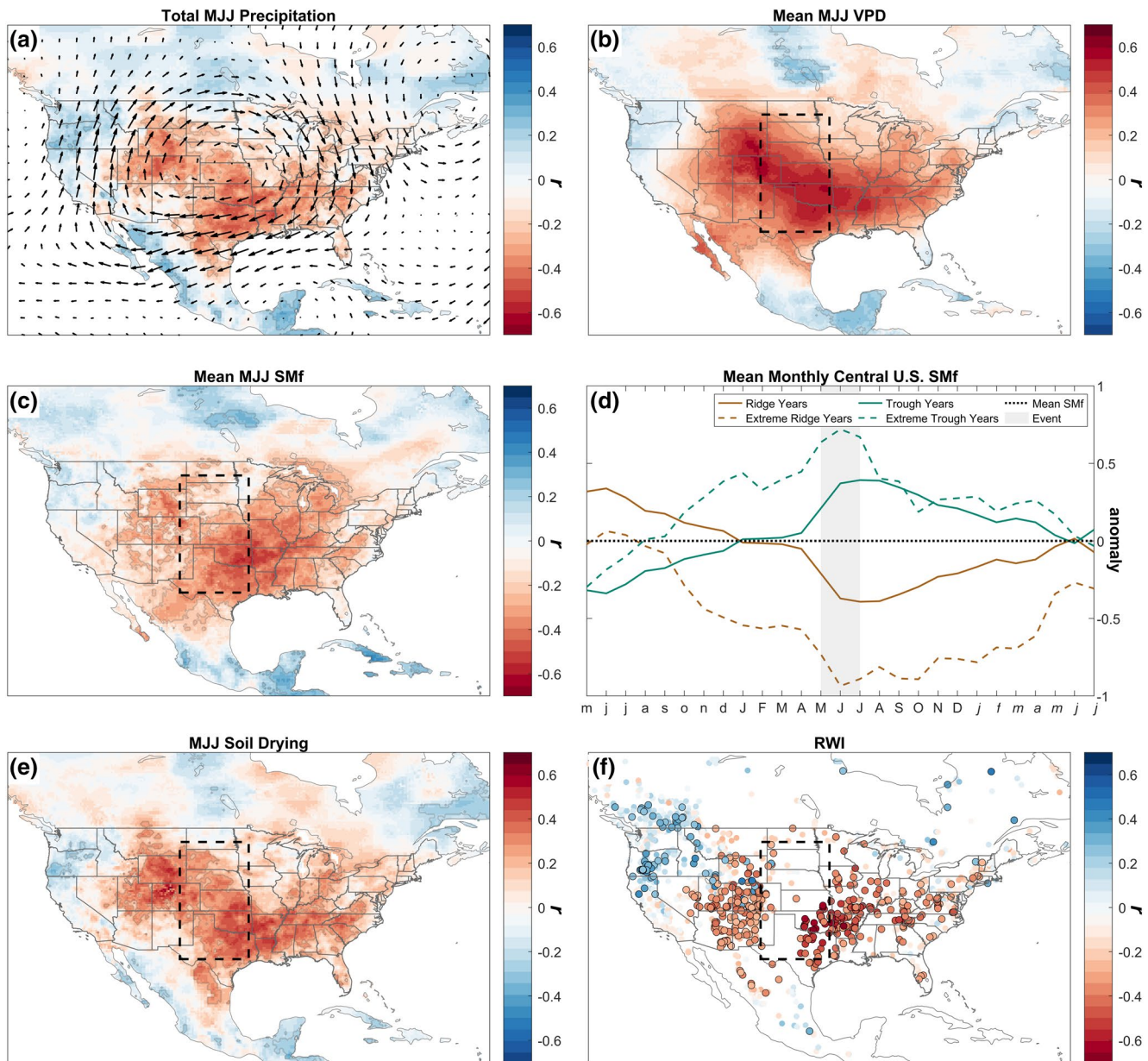


Figure 1. Relationship between May–July (MJJ) mid-tropospheric ridging anomalies over central North America and features of flash droughts. (a)–(c) Correlation (r) between the ridging index and MJJ (a) total precipitation, (b) mean vapor-pressure deficit (VPD), and (c) fraction of mean 0–200 cm soil moisture (SMf). In (a), black arrow vectors indicate correlation between the ridging index and mean 500–700 hPa zonal and meridional wind velocities. (d) Composites of standardized monthly SMf anomalies in years when the standardized MJJ ridging index anomaly was $>1\sigma$ (ridge years), >95 th percentile (exceptional ridge years), $<-1\sigma$ (trough years), and <5 th percentile (exceptional trough years). Gray shading indicates the MJJ period when ridging is evaluated. (e), (f) Correlation between MJJ ridging index and (e) April–July soil drying and (f) tree-ring width index (RWI) chronologies. In (a)–(e), significant ($p < 0.05$) regions are outlined with a gray dotted line. In (f), significant ($p < 0.05$) correlations are shown with circles with black boundaries. The central U.S. (30° – 47° N, 95° – 105° W) is outlined with a black dashed line, and red colors indicate dry conditions.

is that month's mean 0–200 cm soil moisture (plus any snow water equivalent) divided by that month's long-term mean during 1979–2010. The precipitation, VPD, and SMf data were developed by Williams, Anchukaitis, et al. (2020) and are described in detail in that paper's Methods section. A soil drying metric is calculated by first subtracting July SMf from April SMf and then removing the regression-based expected effect of April SMf on this April-to-July difference. A positive soil drying value indicates more drying than expected.

2.3. Atmospheric Ridging Index

We use reanalysis records of atmospheric circulation to develop an MJJ atmospheric ridging index for 1948–2020 (Kalnay et al., 1996). We calculate the ridging index as the mean of five standardized time series: MJJ 600 hPa geopotential heights and 500–700 hPa wind velocities consistent with anti-cyclonic flow around the ridge (Figure S1). These metrics were determined through exploratory analysis to strongly co-vary with mid-continental atmospheric ridging and MJJ soil drying in the central U.S. A positive value of the ridging index indicates the strength of an anomalous ridge, whereas a negative value is indicative of a trough.

2.4. Flash Droughtiness Index

While seasonal resolution is too coarse to allow for direct assessment of rapid drought onset *caused* by ridging, ridging is known to promote drought intensification and thus, years with coincident spring-summer ridging and dry soils can be interpreted as, at the least, flash drought-like. The degree to which a year exhibits flash drought-like conditions is therefore assessed as a combination of how positive and negative that year's ridging and SMf anomalies are, respectively. We use the ridging index and SMf to calculate a “Flash Droughtiness Index” (FDI) as the similarity, or likeness, between a given year's flash drought coordinates (e.g., ridging index = 1σ , SMf = -1σ) and an idealized case of unprecedented flash drought (ridging index = 3σ , SMf = -3σ ; Figure S2). Likeness of a given year to the idealized flash-drought case is calculated as:

$$FDI_y = -\sqrt{(RI_y - 3)^2 + (SMf_y - (-3))^2} \quad (1)$$

where RI is the ridging index anomaly and subscript y specifies the year.

2.5. Standardization and Thresholds of Interest

Observed time series of the ridging index, SMf, and FDI are standardized relative to their common period of 1948–2020. All reconstructions are standardized to match the observed means and standard deviations during their period of overlap with observations.

For SMf, the ridging index, and the FDI, we define moderate anomalies as $\pm 1\sigma$. We designate exceptional anomalies when the variable of interest exceeds the 5th/95th percentile of 1948–2020 observations. Moderate and exceptional flash drought-like conditions are inferred when the FDI exceeds 1σ and the 95th percentile, respectively.

2.6. Tree-ring Network and Reconstruction

Reconstructions of MJJ ridging and central U.S. SMf are produced from an updated version of the North American network of standardized chronologies of ring-width indices (RWI) developed by E. R. Cook et al. (2010). Each RWI chronology is produced from multiple (10+) cross-sections of annual tree rings from a site, detrended for age-dependent or biological growth effects unrelated to climate, and standardized using the “signal free” approach (Melvin & Briffa, 2008).

We use principal components regression (PCR) to reconstruct the MJJ ridging index and 1701° gridded records of SMf across the central U.S. The reconstruction methods are consistent with those established for RWI-based drought atlases (e.g., Cook et al., 1999, 2010, 2015) and Williams, Anchukaitis, et al. (2020), and were recently described in detail by Williams, Cook, et al. (2020). For each reconstruction of gridded SMf, we only consider RWI chronologies within 600 km of the grid cell's center, consistent with E. R. Cook et al. (2010). For reconstruction of the ridging index, we do not impose a distance rule, as atmospheric ridging is a near-continental-scale circulation feature with far-reaching impacts on surface conditions that may be reflected in RWI records across the continent. Initially, both reconstructions are produced allowing all available RWI chronologies with continuous coverage for at least 1800–1983 as possible predictors. To ensure that any correlation between the reconstructions of the ridging index and SMf is not an artifact of common RWI chronologies used by both reconstructions, each RWI chronology that is initially selected by

both reconstruction models is reassigned to only reconstruct the target variable with which it correlates best. The final reconstructions of the ridging index and gridded SMf are based on 100 and 598 independent RWI chronologies, respectively. Finally, a regionally averaged central U.S. SMf reconstruction is calculated and re-standardized.

Model skill is evaluated by the coefficient of determination (R^2) using a k -fold cross-validation approach. This is achieved by reproducing a series of reconstructions, each time withholding k consecutive years from the model calibration period and using the new reconstruction model to estimate the k out-of-sample reconstruction values until all years in the original model's calibration period are assigned out-of-sample values. A cross-validated R^2 is calculated by correlating the time series of out-of-sample reconstruction estimates against the target time series. For the circulation time series (calibration period: 1948–1983), $k = 3$; for the SMf time series (calibration period: 1901–1983), $k = 6$.

2.7. Spectral Analyses

We examine the temporal features of the MJJ ridging index and SMf anomalies using Blackman-Tukey spectra, wavelet coherence (Grinsted et al., 2004) and the data-adaptive method singular spectrum analysis (SSA; Ghil, 1997; Groth & Ghil, 2015; Vautard & Ghil, 1989; Vautard et al., 1992), which has been successfully applied to tree-ring based reconstructions (e.g., Cook et al., 1997, 1998). Whereas SSA provides robust estimates of harmonic components in a time series without *a priori* information, there is an element of subjectivity in determining the optimal embedding window (M) for calculating covariance and the number of “true” signals in the time series (Cook et al., 1998). Therefore, we repeat the SSA several times with varying M to assess the stability of components. We consider a component to be stable if it arises in the top 10 of all reconstructed components, ranked by explained variance, in at least five of the seven M tested. Ultimately, we produce aggregate signals from the range of M where stable components are cleanly extracted to represent the best estimate of the signal.

3. Results and Discussion

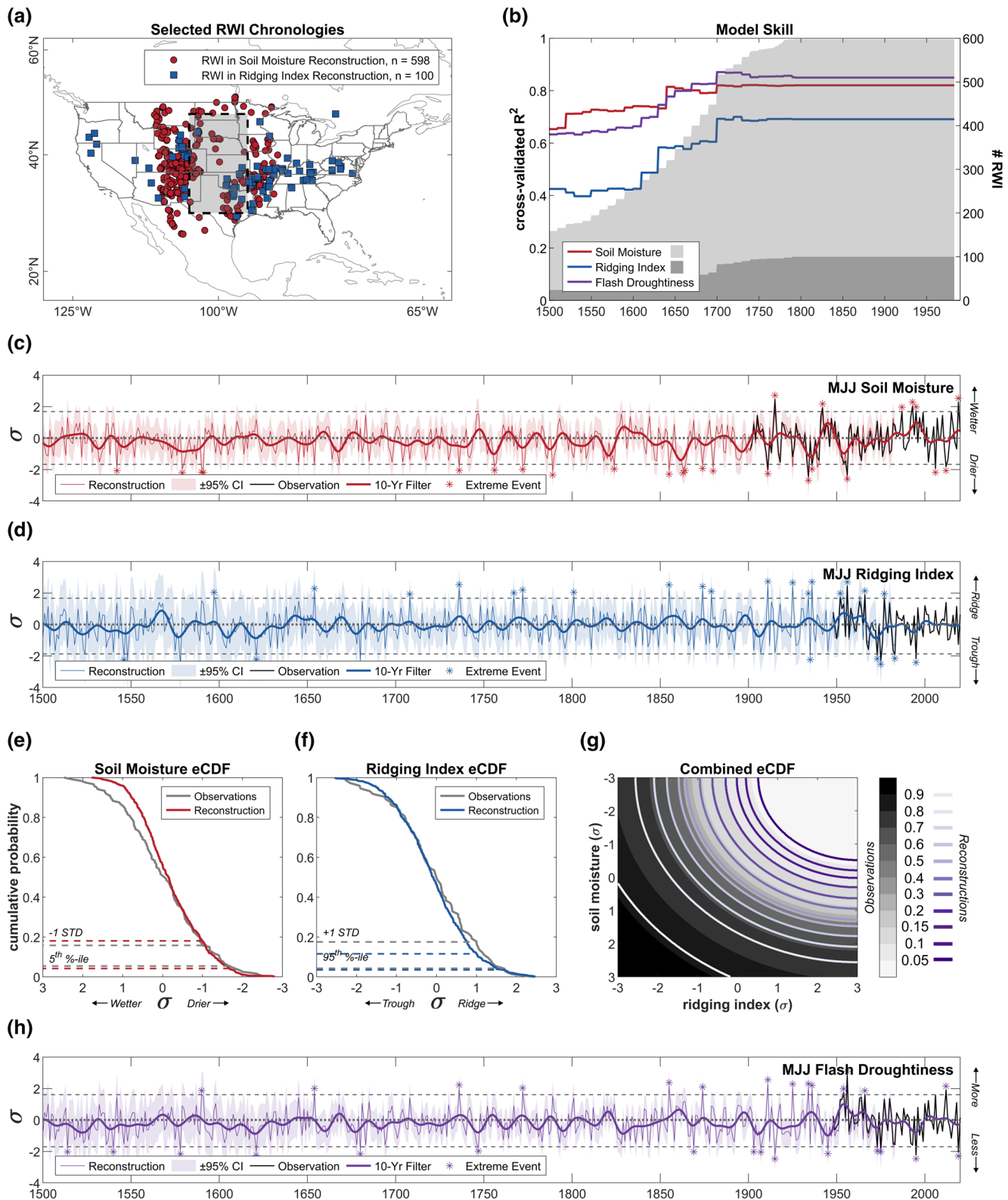
3.1. Observed Variability of Recurring Flash Drought Features, 1948–2020

The variability of MJJ mid-tropospheric ridging anomalies and surface climate conditions that determine water availability are strongly correlated in the central U.S. (Figure 1), consistent with previous analyses (cf. Basara & Christian, 2018; Chen et al., 2019; Seager et al., 2019). An MJJ ridge over interior North America causes precipitation deficits (Figure 1a), enhanced atmospheric evaporative demand (Figure 1b), and reduced soil moisture (Figure 1c). When an MJJ ridge occurs, Great Plains regional SMf—which can be near-normal through April—rapidly decreases over MJJ (Figure 1d). There is good spatial agreement between mean MJJ SMf deficits and the rate of April–July soil drying in the central U.S. (Figures 1c and 1e). Relating the MJJ ridging index to records of RWI across North America reveals a strong and far-reaching correlation fingerprint, with negative correlations with RWI beneath the heart of the mid-continental ridge across the central U.S. and northern Mexico and positive correlations northwest of the ridge in the Pacific Northwest, as well as in the northeastern U.S. and eastern Canada (Figure 1f).

3.2. Reconstructed Atmospheric Ridging, Soil Moisture and Flash Droughtiness, 1500–1983

Figure 2a shows the locations of the independent networks of RWI chronologies used to reconstruct the ridging index and SMf, which are in turn used to calculate the FDI. Cross-validated model skill (R^2) is 0.83, 0.75, and 0.85 for the SMf, ridging index and FDI reconstructions, respectively, back to approximately 1700 (Figure 2b). Prior to 1700, model skill reduces due to decreasing availability of long RWI chronologies. The R^2 of the ridging index reconstruction remains above the 0.5 threshold back to 1600 but only decreases to 0.48 back to 1500, so 1500 is treated as the first-year of our reconstructions.

There is a robust negative relationship between reconstructed interannual ($r = -0.51$, $p < 0.01$) and decadal ($r = -0.41$, $p < 0.01$) variability of MJJ regionally averaged central U.S. SMf and the ridging index over



1500–1983 (Figures 2c and 2d). Periods of persistent ridging and clusters of exceptional individual ridge years coincide with well-documented droughts, such as the late 16th century megadrought (e.g., Stahle et al., 2000), the mid-19th century Civil War drought (e.g., Herweijer et al., 2006), and the 20th century droughts of record

during the 1930s and 1950s (Cook et al., 2011; Williams et al., 2017). The long-term reconstructed probabilities of moderate and exceptional SMf and ridging index anomalies since 1500 are nearly indistinguishable from observational records (Figures 2e and 2f). The probability that moderate negative SMf and positive ridging anomalies coincide is 12.2% in the reconstructions, versus 16.4% in observations; the reconstructed probability of co-occurring exceptional anomalies is 2.1%, versus 1.4% observed (Figure 2g). Uncertainty in tail risk is high, and the higher frequency of exceptional events in the reconstruction is not significantly different from the observed frequency ($p > 0.05$). Although the reconstructions and observations are similar in terms of long-term mean frequencies of co-occurring negative SMf and positive ridging index anomalies, there is substantial centennial variability in the frequency and severity in flash-drought conditions throughout the reconstructed period, indicating the probability of moderate and exceptional events is not consistent from century to century.

Over the last five centuries, flash droughts of at least moderate severity ($>1\sigma$) are inferred in $\sim 17\%$ of years overall ($n = 85$) based on the FDI (Figure 2h and Table S1). Exceptional (>95 th percentile) FDI years occurred in 23 of the last 520 years, the top five of which were in: 1654, 1855, 1911, 1936, and 1956. Several of these years are documented in historical records and associated with catastrophic societal impacts. For instance, the summer of 1855 was recorded as the “Summer of Sitting” in pictographs by Little Bear of the Kiowa in southern Kansas and western Oklahoma due to the extreme heat and widespread vegetation mortality (Gallo & Wood, 2015). The severe drought conditions of that period are considered as a potential factor in the ultimate demise of bison herds in the western U.S. (Woodhouse et al., 2002). Similarly, 1956 has been identified as the worst year of the 1950s Southwest Drought (Cook et al., 2007), the most severe drought on record in the southern and central Great Plains (Schubert et al., 2004), and the second most extensive North American drought year in the past millennium after 1934 (Cook et al., 2014).

A comparison of $>1\sigma$ FDI events by century suggests an increased frequency of moderate and exceptional flash drought-like events from the end of the 16th century megadrought to the mid-20th century. Of the last five centuries, over half of all inferred flash droughts occurred between the mid-1800s and the mid-1900s. Relating the FDI to ridging and SMf (Figures 2c–2d, and 2h), it is clear that the increase in flash-drought frequency from the early 1800s to the mid-1900s is driven by increased frequency of atmospheric ridging years. This period also saw increased frequency of negative FDI and negative ridging (troughing) anomalies, indicating that the increase in flash drought-like years was driven by enhanced variability of atmospheric ridging rather than a positive trend in mean ridging conditions. Indeed, the strongest correlation between FDI and ridging index anomalies of all 73-year periods (the length of the observed record) occurs from 1866 to 1938 ($r = 0.93$, $p < 0.01$). This follows an abnormally quiescent period in the ridging index from the late 1700s to the mid-1800s (Figure 2d) when the FDI is dominated by SMf variability ($r = -0.91$, $p < 0.01$ during 1789–1861). Flash-drought risk varies widely from century to century, suggesting that it is largely by chance that the observed distributions of SMf, ridging index, and FDI anomalies are consistent with those of the five-century reconstruction.

3.3. Spectral Analysis

The observed and reconstructed records of atmospheric ridging suggest it is largely a white noise process, but significant spectral peaks are nonetheless identified at 2 years in observations, and 3.3, 3.66, 5.7, and 7.8 years in the reconstructions (Figure 3a). However, the ridging index spectra were not consistent across the last five centuries (Figures 3b and 3c). The only significant peak shared across multiple centuries is the 7.8-year periodicity (Figure 3b), which was most pronounced in the late 1500s and mid- to late-1800s (Figure 3c). The stable reconstructed components (RCs) extracted with the SSA correspond to the five spectral-peak frequencies and account for 25% of ridging-index variance over the last five centuries, with the

Figure 2. Reconstructed May–July (MJJ) mid-tropospheric ridging and central U.S. soil moisture anomalies since 1500. (a) Distribution of the independent networks of tree-ring width index (RWI) chronologies used in each reconstruction (gray box: region reconstructed for central U.S. soil moisture). (b) Reconstruction model skill (R^2) and the number of RWI chronologies used in each year of the reconstruction. (c) Reconstructed and observed annual (thin line) and decadal (thick line) central U.S. regionally averaged MJJ fraction of mean 0–200 cm soil moisture (SMf; shading: $\pm 95\%$ confidence intervals, dashed lines and stars: 5th and 95th percentiles and individual values exceeding these thresholds). (d) Same as (c), but for the MJJ ridging index. (e), (f) Empirical cumulative distribution function (eCDF) of observed (1948–2020) and reconstructed (1500–1983) MJJ (e) soil moisture and (f) ridging index. (g) Combined eCDF estimate of observed and reconstructed MJJ ridging and SMf associated with flash drought conditions. (h) Same as (c) but for MJJ Flash Droughtiness Index.

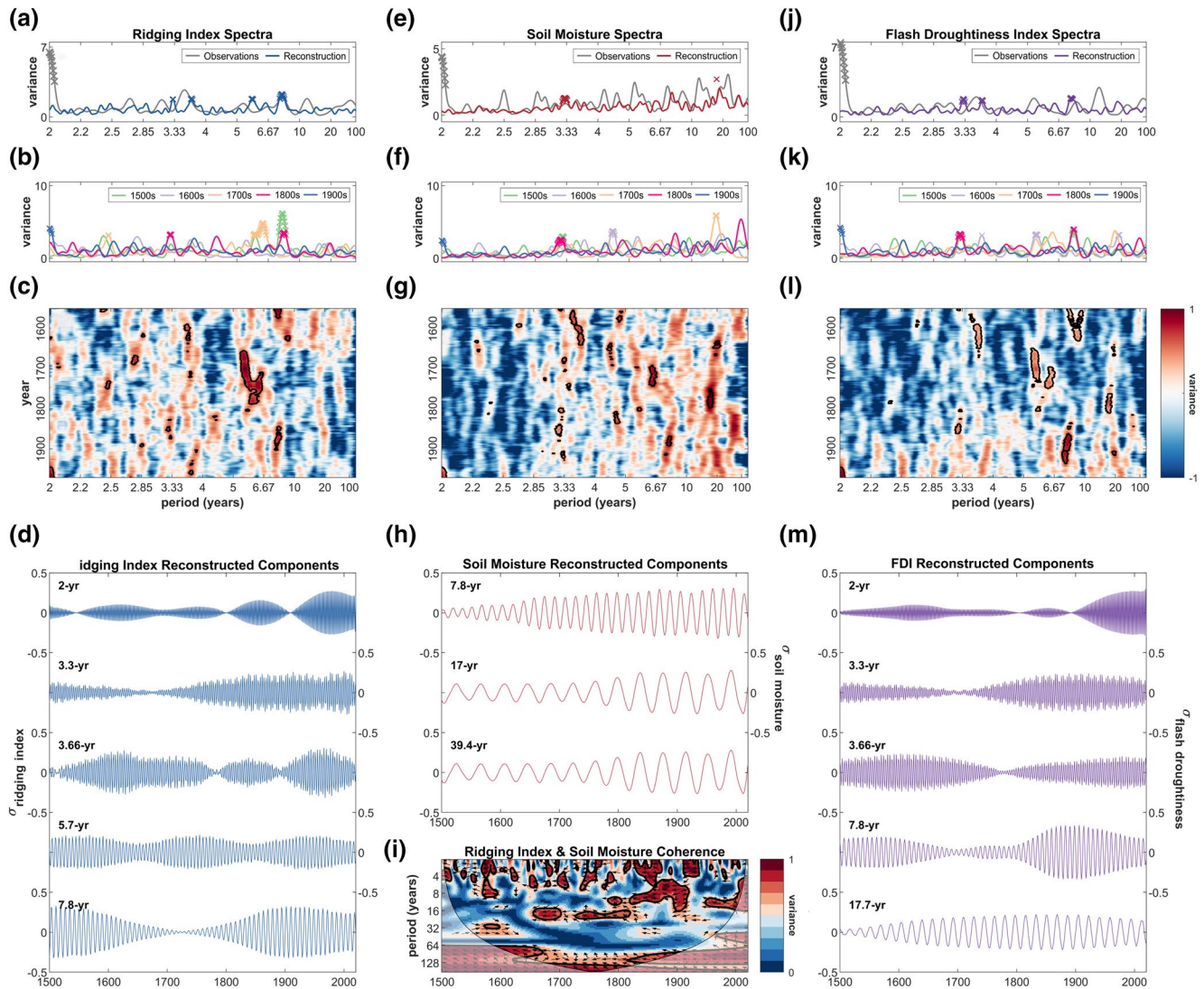


Figure 3. Spectral properties of May–July (MJJ) mid-tropospheric ridging, central U.S. soil moisture, and Flash Droughtiness Index (FDI) anomalies since 1500. (a) Spectra of observed (1948–2020) and reconstructed (1500–1983) MJJ ridging index. (b) Spectra of the MJJ ridging index during each century of the reconstruction. (c) 100-year moving window spectra with y-axis values representing the center year of each 100-year period. Crosses in (a), (b) and black contours in (c) indicate significant (95%) difference from white noise. (d) Reconstructed components (RCs) from singular spectrum analysis of the MJJ ridging index time series. (e)–(h) As for (a)–(d) but for MJJ central U.S. soil moisture anomalies. (i) Wavelet coherence of MJJ ridging and central U.S. soil moisture anomalies between 1500 and 2020. (j–m) As for (a)–(d) but for MJJ FDI.

greatest contribution from the 7.8-year periodicity (Figure 3d). There is a marked increase in the amplitude of the 2-year periodicity since the turn of the 20th century, whereas the amplitude of the 3.3–3.6- and 5.7-year components are relatively steady (Figure 3d).

Like the ridging index, central U.S. SMf anomalies exhibit significant spectral peaks at 2- and 3.3-year periodicities (Figure 3e). A third spectral peak is identified at 17 years, most significant during the 1700s (Figures 3f and 3g). Though the most consistent periodicity occurs around 3–4 years, most of the variance in SMf is concentrated in the lower frequencies (Figure 3g), likely because soil moisture integrates hydroclimate across multiple seasons, including the cool season when teleconnections to ocean temperatures are stronger (Seager et al., 2019). This is supported by the SSA, as the dominant RCs represent 7.9-, 17-, and 39.4-year periodicities (Figure 3h) that together account for 22% of SMf variance, half of which is attributed to the 7.9-year periodicity.

The unique spectral behavior of our independent reconstructions of central U.S. SMf and atmospheric ridging reinforces that these two reconstructions indeed capture unique processes. The antiphase relationship between the two phenomena is strongly localized over periodicities less than ~ 20 years since 1500, though the strength and significance of coherence in variance fluctuates over the study period (Figure 3i).

The timing and strength of concomitant ridging and SMf anomalies indicated by the FDI mirror the leading cycles from both the ridging index and SMf (Figure 3j–m). The significant ($p < 0.05$) peaks and stable RCs center on five periodicities that combine to account for 23% of variance in the FDI reconstruction: 2, 3.3, 3.66, 7.8, and 17 years, with the 7.8-year periodicity accounting for the most variance. The ridging-driven increases in FDI variability and frequency of flash drought-like events from the early 1800s to mid-1900s are associated with an enhanced amplitude of the 7.8-year periodicity, which is apparent in both the ridging and SMf reconstructions.

We note that the extracted RCs are not necessarily true periodic components, but could rather represent stochastic oscillations. However, the multi-centennial stability of 3.3–3.6- and 7.8-year periodicities in the FDI suggests potential for those cycles to aid predictability of the circulation anomalies that promote flash droughts. Furthermore, continued evidence for a low-frequency forcing on central U.S. hydroclimate adds to motivation to better understand the mechanisms responsible for sustaining the North American megadroughts of the medieval period and the late 16th century (Baek et al., 2019; Cook et al., 2018; Seager et al., 2008; Stahle et al., 2000, 2020; Steiger et al., 2019). In particular, our reconstruction suggests that the late 16th century megadrought occurred under persistently strong MJJ atmospheric ridging conditions dominated by the 7.8-year periodicity (Figures 3b–3d), with infrequent, weak troughing and frequent, exceptional ridging events (Figure 2d) associated with five exceptional FDI years (Figure 2h).

4. Conclusions

Our novel tree-ring reconstructions of mid-continental atmospheric ridging provide an unprecedented centuries-long record of the temporal variability of the atmospheric feature most important to flash drought development over the agriculturally productive central U.S. region. This reconstruction is critical because reanalysis-based records of atmospheric circulation are too short and uncertain for confident assessment of the full range of variability of spring-summer ridging anomalies. Our independent reconstruction of central U.S. spring-summer soil moisture then allows for identification of likely flash drought years, when strong atmospheric ridging coincided with reduced growing-season soil moisture. While the records of annual tree-ring widths used in this study are too coarse for direct reconstruction of rapid drought onset *caused* by ridging, ridging is known to promote drought intensification and thus, years with coincident spring-summer ridging and dry soils can be interpreted as, at the least, flash drought-like.

These reconstructions and our resultant reconstruction of a FDI indicate that our short observation-based records of these variables are actually good representations of the long-term probabilistic distribution of flash-drought anomalies in the central U.S. However, this result may be coincidental, as our reconstruction reveals that the risks of exceptional atmospheric ridging anomalies and flash droughts have not been stable over time. For example, our observational record of FDI begins in the mid-1900s at what our reconstruction indicates was a point of high flash-drought frequency on the tail end of a unique increase in atmospheric ridging variability that began in the early 1800s. The reconstructions also indicate relatively stable periodicities in flash droughtiness of 3.3–3.6 and 7.8 years, akin to the ridging index. This suggests that interannual variability in spring-summer ridging is not a purely random white-noise process, and more work should be done to evaluate whether these periodicities arise from sources of untapped predictive skill. These results may guide future work to diagnose the roles of external, oceanic, and land-surface forcing of warm-season atmospheric circulation and hydroclimate over North America.

Data Availability Statement

Data used in this study can be accessed at <https://www.ldeo.columbia.edu/~williams/flashdrought/>. Reanalysis climate data come from <https://psl.noaa.gov/data/gridded/data.ncep.reanalysis.html>.

Acknowledgments

The authors are grateful to the many contributors to the International Tree-Ring Databank, without which this work would not be possible. Thank you to Andy Bunn and Jeremy Littell for sharing several records of tree-ring width from the Pacific Northwest region of the United States. Funding was provided by NSF AGS-1703029 (KCB, APW, ERC), NASA 16-MAP16-0081 (APW, BIC), and NOAA MAPP NA19OAR4310278 (APW, BIC).

References

- Baek, S. H., Smerdon, J. E., Seager, R., Williams, A. P., & Cook, B. I. (2019). Pacific Ocean forcing and atmospheric variability are the dominant causes of spatially widespread droughts in the contiguous United States. *Journal of Geophysical Research: Atmospheres*, *124*, 2507–2524. <https://doi.org/10.1029/2018JD029219>
- Basara, J. B., & Christian, J. I. (2018). Seasonal and interannual variability of land-atmosphere coupling across the Southern Great Plains of North America using the North American regional reanalysis: Seasonal and interannual variability of land-atmosphere coupling. *International Journal of Climatology*, *38*, 964–978. <https://doi.org/10.1002/joc.5223>
- Basara, J. B., Christian, J. I., Wakefield, R. A., Otkin, J. A., Hunt, E. H., & Brown, D. P. (2019). The evolution, propagation, and spread of flash drought in the Central United States during 2012. *Environmental Research Letters*, *14*, 084025. <https://doi.org/10.1088/1748-9326/ab2cc0>
- Basara, J. B., Maybourn, J. N., Peirano, C. M., Tate, J. E., Brown, P. J., Hoey, J. D., et al. (2013). Drought and associated impacts in the great plains of the United States—A review. *International Journal of Geosciences*, *04*, 72–81. <https://doi.org/10.4236/ijg.2013.46A2009>
- Chen, L. G., Gottschalk, J., Hartman, A., Miskus, D., Tinker, R., & Artusa, A. (2019). Flash drought characteristics based on U.S. drought monitor. *Atmosphere*, *10*(9), 498. <https://doi.org/10.3390/atmos10090498>
- Christian, J. I., Basara, J. B., Hunt, E. D., Otkin, J. A., & Xiao, X. (2020). Flash drought development and cascading impacts associated with the 2010 Russian heatwave. *Environmental Research Letters*, *15*, 094078. <https://doi.org/10.1088/1748-9326/ab9faf>
- Christian, J. I., Basara, J. B., Otkin, J. A., & Hunt, E. D. (2019). Regional characteristics of flash droughts across the United States. *Environmental Research Communications*, *1*, 125004. <https://doi.org/10.1088/2515-7620/ab50ca>
- Christian, J. I., Basara, J. B., Otkin, J. A., Hunt, E. D., Wakefield, R. A., Flanagan, P. X., et al. (2019). A methodology for flash drought identification: Application of flash drought frequency across the United States. *Journal of Hydrometeorology*, *20*, 833–846. <https://doi.org/10.1175/JHM-D-18-0198.1>
- Cook, E. R., D'Arrigo, R. D., & Briffa, K. R. (1998). A reconstruction of the North Atlantic Oscillation using tree-ring chronologies from North America and Europe. *The Holocene*, *8*(1), 9–17. <https://doi.org/10.1191/09596839867793725>
- Cook, E. R., Kushnir, Y., Smerdon, J. E., Williams, A. P., Anchukaitis, K. J., & Wahl, E. R. (2019). A Euro-Mediterranean tree-ring reconstruction of the winter NAO index since 910 C. *Climate Dynamics*, *53*, 1567–1580. <https://doi.org/10.1007/s00382-019-04696-2>
- Cook, B. I., Mankin, J. S., Marvel, K., Williams, A. P., Smerdon, J. E., & Anchukaitis, K. J. (2020). Twenty-first Century Drought Projections in the CMIP6 Forcing Scenarios. *Earth's Future*, *8*, e2019EF001461. <https://doi.org/10.1029/2019EF001461>
- Cook, E. R., Meko, D. M., Stahle, D. W., & Cleaveland, M. K. (1999). Drought reconstructions for the continental United States. *Journal of Climate*, *12*(4), 1145–1162. [https://doi.org/10.1175/1520-0442\(1999\)012<1145:DRFTCU>2.0.CO;2](https://doi.org/10.1175/1520-0442(1999)012<1145:DRFTCU>2.0.CO;2)
- Cook, E. R., Meko, D. M., & Stockton, C. W. (1997). A new assessment of possible solar and lunar forcing of the bidecadal drought rhythm in the western United States. *Journal of Climate*, *10*(6), 1343–1356. [https://doi.org/10.1175/1520-0442\(1997\)010<1343:ANAO PS>2.0.CO;2](https://doi.org/10.1175/1520-0442(1997)010<1343:ANAO PS>2.0.CO;2)
- Cook, E. R., Seager, R., Cane, M. A., & Stahle, D. W. (2007). North American drought: Reconstructions, causes, and consequences. *Earth-Science Reviews*, *81*, 93–134. <https://doi.org/10.1016/j.earscirev.2006.12.002>
- Cook, E. R., Seager, R., Heim, R. R., Vose, R. S., Herweijer, C., & Woodhouse, C. (2010). Megadroughts in North America: Placing IPCC projections of hydroclimatic change in a long-term paleoclimate context. *Journal of Quaternary Science*, *25*, 48–61. <https://doi.org/10.1002/jqs.1303>
- Cook, E. R., Seager, R., Kushnir, Y., Briffa, K. R., Büntgen, U., Frank, D., et al. (2015). Old World megadroughts and pluvials during the Common Era. *Science Advances*, *1*, e1500561. <https://doi.org/10.1126/sciadv.1500561>
- Cook, B. I., Seager, R., & Miller, R. L. (2011). Atmospheric circulation anomalies during two persistent North American droughts: 1932–1939 and 1948–1957. *Climate Dynamics*, *36*, 2339–2355. <https://doi.org/10.1007/s00382-010-0807-1>
- Cook, B. I., Seager, R., & Smerdon, J. E. (2014). The worst North American drought year of the last millennium: 1934. *Geophysical Research Letters*, *41*, 7298–7305. <https://doi.org/10.1002/2014GL061661>
- Cook, B. I., Williams, A. P., Smerdon, J. E., Palmer, J. G., Cook, E. R., Stahle, D. W., et al. (2018). Cold tropical Pacific Sea surface temperatures during the late sixteenth-century North American megadrought. *Journal of Geophysical Research: Atmospheres*, *123*, 11307–11320. <https://doi.org/10.1029/2018JD029323>
- Cowan, T., Hegerl, G. C., Colfescu, I., Bollasina, M., Purich, A., & Boschat, G. (2017). Factors contributing to record-breaking heat waves over the great plains during the 1930s dust bowl. *Journal of Climate*, *30*(7), 2437–2461. <https://doi.org/10.1175/JCLI-D-16-0436.1>
- Fritts, H. C. (1976). *Tree rings and climate*, New York, NY: Academic Press.
- Gallo, K., & Wood, E. (2015). Historical drought events of the Great Plains recorded by native Americans. *Great Plains Research*, *25*, 151–158. <https://doi.org/10.1353/gpr.2015.0035>
- Ghil, M. (1997). The SSA-MTM Toolkit: Applications to analysis and prediction of time series. *Proceedings of SPIE*, *3165*, 216–230. <https://doi.org/10.1117/12.279594>
- Grinsted, A., Moore, J. C., & Jevrejeva, S. (2004). Application of the cross wavelet transform and wavelet coherence to geophysical time series. *Nonlinear Processes in Geophysics*, *11*, 561–566. <https://doi.org/10.5194/npg-11-561-2004>
- Groth, A., & Ghil, M. (2015). Monte carlo singular spectrum analysis (SSA) revisited: Detecting oscillator clusters in multivariate datasets. *Journal of Climate*, *28*, 7873–7893. <https://doi.org/10.1175/JCLI-D-15-0100.1>
- Herweijer, C., Seager, R., & Cook, E. R. (2006). North American droughts of the mid- to late-nineteenth century: A history, simulation and implication for Medieval drought. *The Holocene*, *16*, 159–171. <https://doi.org/10.1191/0959683606hl917rp>
- Hodges, D., & Pu, Z. (2019). Characteristics and variations of low-level jets and environmental factors associated with summer precipitation extremes over the Great Plains. *Journal of Climate*, *32*, 5123–5144. <https://doi.org/10.1175/JCLI-D-18-0553.1>
- Hoerling, M., Eischeid, J., Kumar, A., Leung, R., Mariotti, A., Mo, K., et al. (2014). Causes and predictability of the 2012 Great Plains drought. *Bulletin of the American Meteorological Society*, *95*, 269–282. <https://doi.org/10.1175/BAMS-D-13-00055.1>
- Howard, I. M., Stahle, D. W., & Feng, S. (2018). Separate tree-ring reconstructions of spring and summer moisture in the northern and southern Great Plains. *Climate Dynamics*, *52*, 5877–5897. <https://doi.org/10.1007/s00382-018-4485-8>
- Kalnay, E., Kanamitsu, M., Kistler, R., Collins, W., Deaven, D., Gandin, L., et al. (1996). The NCEP/NCAR 40-year reanalysis project. *Bulletin of the American Meteorological Society*, *77*(3), 437–471. [https://doi.org/10.1175/1520-0477\(1996\)077<0437:TNYRP>2.0.CO;2](https://doi.org/10.1175/1520-0477(1996)077<0437:TNYRP>2.0.CO;2)
- Koster, R. D., Chang, Y., & Schubert, S. D. (2014). A mechanism for land-atmosphere feedback involving planetary wave structures. *Journal of Climate*, *27*, 9290–9301. <https://doi.org/10.1175/JCLI-D-14-00315.1>
- Livneh, B., & Hoerling, M. P. (2016). The physics of drought in the U.S. Central Great Plains. *Journal of Climate*, *29*, 6783–6804. <https://doi.org/10.1175/JCLI-D-15-0697.1>

- Lopez, H., Lee, S., Dong, S., Goni, G., Kirtman, B., Atlas, R., et al. (2019). East Asian monsoon as a modulator of U.S. Great Plains heat waves. *Journal of Geophysical Research: Atmospheres*, *124*, 6342–6358. <https://doi.org/10.1029/2018JD030151>
- Melvin, T. M., & Briffa, K. R. (2008). A “signal-free” approach to dendroclimatic standardization. *Dendrochronologia*, *26*, 71–86. <https://doi.org/10.1016/j.dendro.2007.12.001>
- Otkin, J. A., Svoboda, M., Hunt, E. D., Ford, T. W., Anderson, M. C., Hain, C., et al. (2018). Flash droughts: A review and assessment of the challenges imposed by rapid-onset droughts in the United States. *Bulletin of the American Meteorological Society*, *99*, 911–919. <https://doi.org/10.1175/BAMS-D-17-0149.1>
- PaiMazumder, D., & Done, J. M. (2016). Potential predictability sources of the 2012 U.S. drought in observations and a regional model ensemble. *Journal of Geophysical Research: Atmospheres*, *121*, 12581–12592. <https://doi.org/10.1002/2016JD025322>
- Pendergrass, A. G., Meehl, G. A., Pulwarty, R., Hobbins, M., Hoell, A., AghaKouchak, A., et al. (2020). Flash droughts present a new challenge for subseasonal-to-seasonal prediction. *Nature Climate Change*, *10*, 191–199. <https://doi.org/10.1038/s41558-020-0709-0>
- Schubert, S. D., Suarez, M. J., Pegion, P. J., Koster, R. D., & Bacmeister, J. T. (2004). Causes of long-term drought in the U.S. Great Plains. *Journal of Climate*, *17*, 485–503. [https://doi.org/10.1175/1520-0442\(2004\)017<0485:COLDIT>2.0.CO;2](https://doi.org/10.1175/1520-0442(2004)017<0485:COLDIT>2.0.CO;2)
- Seager, R., Burgman, R., Kushnir, Y., Clement, A., Cook, E., Naik, N., et al. (2008). Tropical Pacific forcing of North American medieval megadroughts: Testing the concept with an atmosphere model forced by coral-reconstructed SSTs*. *Journal of Climate*, *21*, 6175–6190. <https://doi.org/10.1175/2008JCLI2170.1>
- Seager, R., Nakamura, J., & Ting, M. (2019). Mechanisms of seasonal soil moisture drought onset and termination in the Southern Great Plains. *Journal of Hydrometeorology*, *20*, 751–771. <https://doi.org/10.1175/JHM-D-18-0191.1>
- Stahle, D. W., Cook, E. R., Burnette, D. J., Torbenson, M. C. A., Howard, I. M., Griffin, D., et al. (2020). Dynamics, Variability, and Change in Seasonal Precipitation Reconstructions for North America. *Journal of Climate*, *33*, 3173–3195. <https://doi.org/10.1175/JCLI-D-19-0270.1>
- Stahle, D. W., Cook, E. R., Cleaveland, M. K., Therrell, M. D., Meko, D. M., Grissino-Mayer, H. D., et al. (2000). Tree-ring data document 16th century megadrought over North America. *Transactions American Geophysical Union*, *81*(12), 121–125. <https://doi.org/10.1029/00EO00076>
- Stahle, D. W., Fye, F. K., Cook, E. R., & Griffin, R. D. (2007). Tree-ring reconstructed megadroughts over North America since AD 1300. *Climatic Change*, *83*, 133–149. <https://doi.org/10.1007/s10584-006-9171-x>
- Steiger, N. J., Smerdon, J. E., Cook, E. R., & Cook, B. I. (2018). A reconstruction of global hydroclimate and dynamical variables over the Common Era. *Scientific Data*, *5*, 180086. <https://doi.org/10.1038/sdata.2018.86>
- Steiger, N. J., Smerdon, J. E., Cook, B. I., Seager, R., Williams, A. P., & Cook, E. R. (2019). Oceanic and radiative forcing of medieval megadroughts in the American Southwest. *Science Advances*, *5*, eaax0087. <https://doi.org/10.1126/sciadv.aax0087>
- Vautard, R., & Ghil, M. (1989). Singular spectrum analysis in nonlinear dynamics, with applications to paleoclimatic time series. *Physica D: Nonlinear Phenomena*, *35*(3), 395–424. [https://doi.org/10.1016/0167-2789\(89\)90077-8](https://doi.org/10.1016/0167-2789(89)90077-8)
- Vautard, R., Yiou, P., & Ghil, M. (1992). Singular-spectrum analysis: A toolkit for short, noisy chaotic signals. *Physica D: Nonlinear Phenomena*, *58*(1–4), 95–126. [https://doi.org/10.1016/0167-2789\(92\)90103-T](https://doi.org/10.1016/0167-2789(92)90103-T)
- Wang, H., Schubert, S. D., Koster, R. D., & Chang, Y. (2019). Phase locking of the boreal summer atmospheric response to dry land surface anomalies in the Northern Hemisphere. *Journal of Climate*, *32*, 1081–1099. <https://doi.org/10.1175/JCLI-D-18-0240.1>
- Williams, A. P., Anchukaitis, K. J., Woodhouse, C. A., Meko, D. M., Cook, B. I., Bolles, K., et al. (2020). Tree rings and observations suggest no stable cycles in Sierra Nevada cool-season precipitation. *Water Resources Research*, *56*, e2020WR028599. <https://doi.org/10.1029/2020WR028599>
- Williams, A. P., Cook, B. I., Smerdon, J. E., Bishop, D. A., Seager, R., & Mankin, J. S. (2017). The 2016 Southeastern U.S. Drought: An extreme departure from centennial wetting and cooling. *Journal of Geophysical Research: Atmospheres*, *122*, 10888–10905. <https://doi.org/10.1002/2017JD027523>
- Williams, A. P., Cook, E. R., Smerdon, J. E., Cook, B. I., Abatzoglou, J. T., Bolles, K. C., et al. (2020). Large contribution from anthropogenic warming to a developing North American megadrought. *Science*, *368*, 314–318. <https://doi.org/10.1126/science.aaz9600>
- Wise, E. K., & Dannenberg, M. P. (2014). Persistence of pressure patterns over North America and the North Pacific since AD 1500. *Nature Communications*, *5*, 4912. <https://doi.org/10.1038/ncomms5912>
- Woodhouse, C. A., Lukas, J. J., & Brown, P. M. (2002). Drought in the western Great Plains, 1845–56: Impacts and implications. *Bulletin of the American Meteorological Society*, *83*, 1485–1494. <https://doi.org/10.1175/BAMS-83-10-1485>
- Woodhouse, C. A., & Overpeck, J. T. (1998). 2000 years of drought variability in the Central United States. *Bulletin of the American Meteorological Society*, *79*(12), 2693–2714. [https://doi.org/10.1175/1520-0477\(1998\)079<2693:YODVIT>2.0.CO;2](https://doi.org/10.1175/1520-0477(1998)079<2693:YODVIT>2.0.CO;2)
- Zhao, S., Deng, Y., & Black, R. X. (2017). Observed and simulated spring and summer dryness in the United States: The impact of the Pacific Sea surface temperature and beyond. *Journal of Geophysical Research: Atmospheres*, *122*(23), 12–713. <https://doi.org/10.1002/2017JD027279>